ACS APPLIED BIO MATERIALS

www.acsabm.org Article

High-Sensitivity 3D ZIF-8/PDA Photonic Crystal-Based Biosensor for Blood Component Recognition

Maryam Nankali, Zahra Einalou, Mohsen Asadnia, and Amir Razmjou*

Cite This: *ACS Appl. Bio Mater.* 2021, 4, 1958–1968 Read Online

ACCESS | Metrics & More | Article Recommendations

ABSTRACT: Optical biosensors are sensitive devices used in bioanalytics detection. Analysis of blood constituents is very important for the detection of major diseases and also performs a significant role in the diagnosis of diabetes, various cancers, and cardiovascular disorders. In this work, a three-dimensional photonic crystal-based biosensor composed of zeolitic imidazolate framework-8 (ZIF-8) nanoarrays are placed on polydopamine (PDA) coated on a silicon substrate. This sensor is designed, simulated, and evaluated for various blood components in the wavelength range of 1.1 to 1.5 μm by the finite-difference time-domain (FDTD) method. The proposed biosensor was used for 10 types of blood components such as biotin−streptavidin, bovine serum albumin (BSA), cytop, glucose (40 mg/100 mL), hemoglobin, blood plasma, Sylgard184, white blood compounds, urethane dimethacrylate, and polyacrylamide. The FDTD technique was used for the performance analysis of the biosensor. The design parameters of the radius, the lattice constant, the thickness of the ZIF-8 arrays, and the PDA layer thickness are chosen to optimize the photonic crystal structure. This study indicates that the thickness of the PDA is the most important parameter for peak wavelength value in comparison to the other physical parameters. The factors for optimizing the photonic crystal-based biosensors such as the peak wavelength value (PWV), sensitivity, full width at half-maximum (FWHM), and figure of merit (FOM) are significant in comparison with pertinent works in this field, which evaluated 171 nm/RIU, 7.62 nm, and 22.5 RIU^{-1}, respectively. A change of 0.01 nm in the refractive index of the constituents of the blood leads to a shift of 80 nm in the maximum peak wavelength, therefore acting as a functional biosensor with a high detection limit of 0.004 RIU.

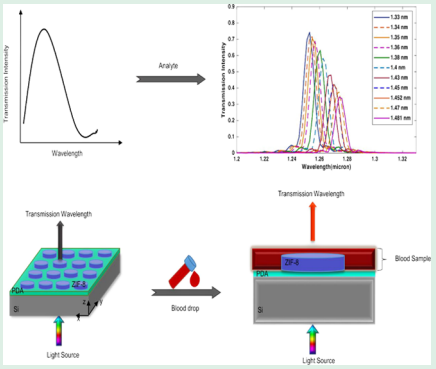

KEYWORDS: *photonic crystal, biosensor, FDTD, zeolitic imidazolate framework-8 (ZIF-8), polydopmaine (PDA)*

1. INTRODUCTION

Blood is a vital liquid made up of various components used for different signs. Knowledge of the optical properties of the blood is not only crucial for any specific diagnostic and therapeutic applications but also essential for common medical diagnoses such as cardiovascular diseases, cancers, and diabetes.[1]

Biosensors are a progress in analytical science, in which their design is based on selective identification of the analysis depending on the physiological components and interactions with physical and chemical detectors.[2−4] There are many kinds of biosensors for the recognition of biochemical interactions, such as electrical, optical, calorimetric, etc.[5] Conventional diagnostic methods in medicine require the use of expensive devices that need costly maintenance to ensure an accurate operation.[6] Among the many types of biosensors, the optical-based biosensors have a reliable detection and an extensive range of applications in various fields such as medical, healthcare, pharmaceuticals, and environmental monitoring. There are two detection methods in photonic biosensors: fluorescence-based identification and label-free recognition. In the primary method, target molecules are marked with fluorescent labels.[7] This method is not appropriate for blood analysis as it is an opaque medium with many interfering compounds. On the other hand, in label-free diagnosis, the target molecules are not marked. The method in blood analysis uses the refractive index of the target sample.[8] Several ways have been reported in optical labeled-free biosensors, as follows: surface plasmon resonance (SPR),[9] interferometer,[10] waveguide,[11] ring resonator,[12] optical fiber,[13] and photonic crystal (PC).[14]

Among photonic biosensors, the photonic crystal-based biosensor is one of the promising platforms for optical data preparation since it allows the effective photonic integration and wide domain incorporation on a chip. These structures

Received: December 8, 2020
Accepted: December 28, 2020
Published: January 20, 2021

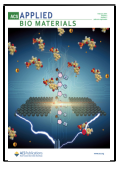

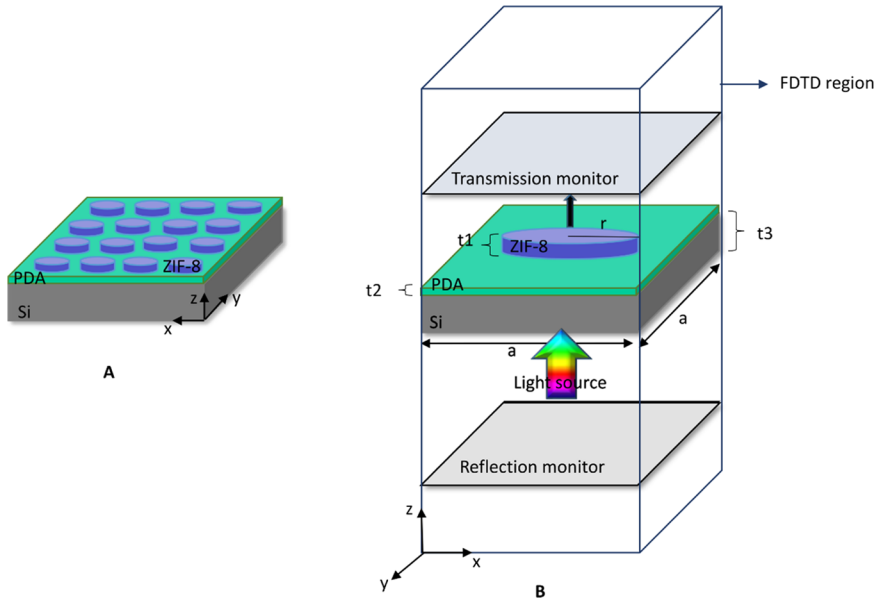

Figure 1. The overall photonic crystal structure in a three-dimensional transect: (A) there are ZIF-8 arrays upon the PDA layer on the Si substrate. In the unit cell (B), there are some parameters such as the lattice constant "*a*" that is 1.5 μm, radius "*r*" of the ZIF-8 array is 600 nm, thickness "*t*1" of the ZIF-8 is 200 nm, and the thickness of PDA layer "*t*2" and Si substrate "*t*3" is 10 nm and 260 nm, respectively. In the FDTD region, there are a plane-wave light under construction (−600 nm), a reflection monitor below the light source (−1.2 μm), and a transmission monitor above the structure (1.2 μm) in the *z*-direction.

with regular dielectric are dependent on the light wavelength.[15] Photonic crystal-based biosensors are a new generation of biosensors that operate as optical transducers,[16] with improved repeatability and reliability of the results.

Many methods have been employed to detect the different components of blood. A 2D PC-based biosensor was proposed for the recognition of blood constituents with finite difference time domain (FDTD), MIT Electromagnetic Equation Propagation (MEEP), and MIT Photonic Bands (MBP), all computer simulation platforms. They are used for spectrum transmission, which alters frequency, as shown in ref 17. A ring resonator has been used for the diagnosis of glucose concentration for urine analysis by using the FDTD and MEEP simulation, in which the *Q* factor and output power are measured.[18] Another biosensor has been proposed as photonic crystal fiber (PCF) for the diagnosis of glucose concentration using a finite element method (FEM), by which only sensitivity can be calculated and the quality factor and other sensor factors are not investigated.[19] Another work has designed the sensing of solid-core photonic crystal fiber (PCF) to detect blood components through the FEM technique to measure the sensitivity and dominate the losses.[20] In another study, a photonic crystal ring resonator has been used to indicate transmission intensity, and the *Q* factor for various types of blood components with different refractive index (RI) and sensitivity has not been calculated.[21] A 2D nanocavity-coupled photonic crystal sensor has been simulated to show the detection of 10 blood components with high quality and sensitivity by the FDTD and plane wave expansion (PWE) methods; however, fabrication is difficult for this design.[22]

Among nanostructured materials with various applications,[23−25] metal−organic frameworks (MOFs) are a new class of nanoporous materials with a large size of cavities, high specific surface area, and selective absorption by small molecules and ions.[26] Their optical and magnetic responses in the presence of guest molecules have various applications in catalysis,[27] storages,[28] and filtration and separation.[29,30] ZIF-8 is a type of MOF composed of zinc ions and 2-methylimidazolate groups. ZIF-8s are porous materials with chemical and thermal stability and adjustable pore size.[31−33] It also has a small pore size (∼3.4 Å) and large cavities (∼11.6 Å in diameter).[34] ZIF-8 is used in various applications such as separation,[35] catalysis,[36] sensing,[37] and drug delivery.[38]

Polydopamine (PDA) is a significant polymer used for different coating surfaces.[39,40] It is organized by the oxidation of dopamine but also has gained increased consideration amid the catechol-containing coats.[41] The PDA coating is a considerable regenerative polymer. It has been used in biomedical applications such as drug delivery,[42] biosensing,[43] and biomolecule immobilization.[44] Recently, a study on PDA has shown that this polymer is very stable and has the ability to regenerate and absorb organic and inorganic molecules.[45]

We previously managed to make photonic crystals based on ZIF-8/PDA patterning,[46] and here we studied the potential of our platform theoretically to be used as a biosensor for the detection of various biomolecules. In this study, a label-free photonic crystal biosensor is proposed consisting of ZIF-8 arrays and PDA coating on a silicon substrate. This procedure is innovative as polydopamine coatings can aid in the growth and formation of thin-film MOFs. This ZIF-8/PDA photonic crystal will be able to lead to serving as a suitable platform for the production of a wide range of biosensors. The proposed biosensor works based on the refractive index change by using various kinds of analytic samples, such as different blood components, leading to a shift in peak wavelength. In this work, 10 variant components of the blood have been examined. The biosensor, consisting of the ZIF-8 arrays and PDA layer, was able to detect these substances. Noticeable factors are a high sensitivity of 171 nm/RIU, low FWHM, and desirable FOM.

https://dx.doi.org/10.1021/acsabm.0c01586
ACS Appl. Bio Mater. 2021, 4, 1958−1968

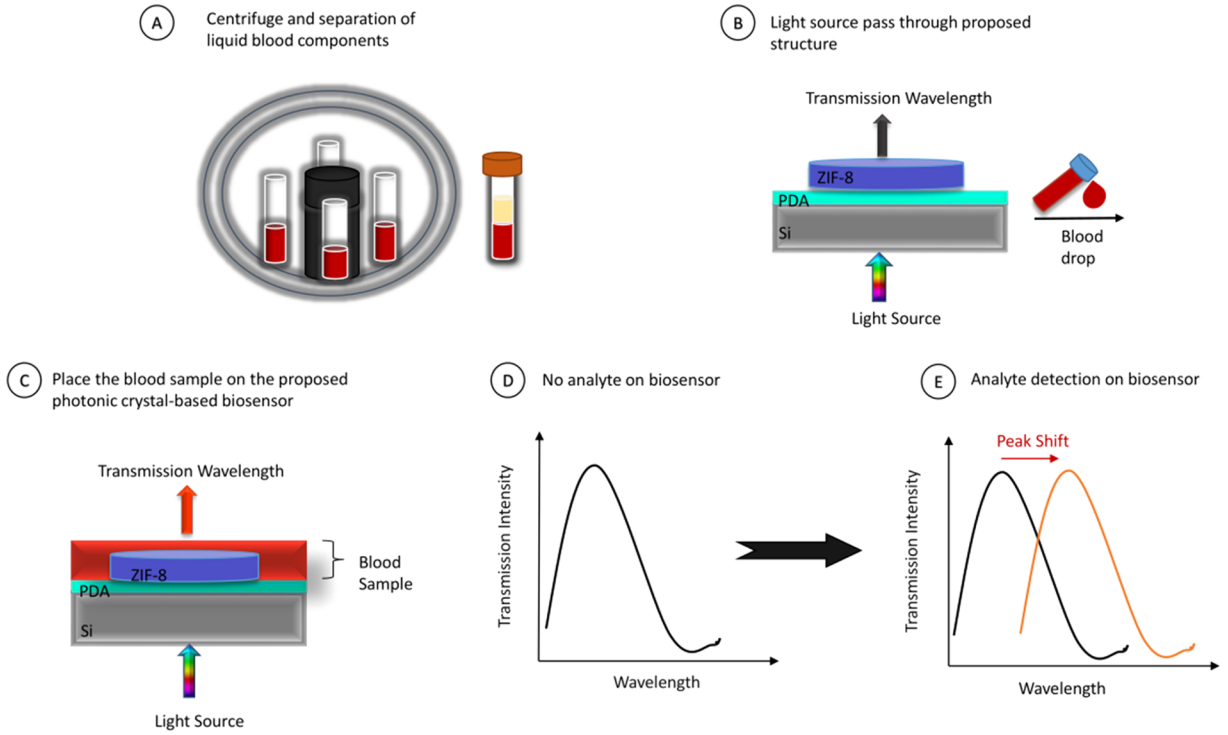

Figure 2. Proposed ZIF-8/PDA photonic crystal-based biosensor for performance: white light passed through the structure and indicated a peak wavelength. Then, blood was dropped on the system for testing the biosensor, which can be seen as the peak wavelength shifted; so detection has occurred.

2. MATERIALS AND METHODS

Sigma-Aldrich provided all solvents and chemicals, including the dopamine hydrochloride, polyethyleneimine, zinc nitrates, and 2-methylimidazole. The AZ 1518 positive photoresist from Micro Chemicals was used in the photolithography procedure. The experiment was done, and a photonic crystal was made as described in our previous work.[46]

2.1. Theory. The refractive index "n" is one of the optical properties of materials, defined as:[47]

$$n = \frac{C}{v} \tag{1}$$

where "c" and "v" show the speeds of light in a vacuum and the environment, respectively. The speed of light in the environment related to the frequency and the wavelength of light, as shown below:

$$\lambda = \frac{v}{f} \tag{2}$$

When light passes through materials, its frequency does not change. So the speed of light and the wavelength are depending on each other, while frequency is constant.

This result is obtained for two different conditions:

$$\frac{n2}{n1} = \frac{\lambda 1}{\lambda 2} \tag{3}$$

Accordingly, we conclude that the refractive index variations are due to the wavelength peak shifts. By placing the sample on the system and following the change in the refractive index, the peak wavelength was shifted. In this field, the refractive index of blood components was used to test the biosensor.[17]

2.2. Sensor Model Design. Photonic crystals are analyzed by solving Maxwell's equations in complex geometries. The finite difference time domain (FDTD) is an advanced, numerical, time-domain method used for electrodynamic modeling.[48−50] In the main, FDTD is used to calculate electromagnetic fields as a function of wavelength/frequency by applying Fourier transforms during simulation. Therefore, beneficial values such as complex polynomial vectors and light transmission/reflection wavelength are calculated. Figure 1 shows a ZIF-8/PDA photonic crystal with the FDTD region for computing the transmission spectrum in perspective view. Figure 1A displays the overview geometry of the suggested PC biosensor. The structure is made up of three layers, including a ZIF-8 array on a thin layer of PDA coated on the silicon substrate. Figure 1B indicates the details in the unit cell; as can be seen, "a" is the lattice constant, "$t1$" is the thickness of the ZIF-8 arrays, "$t2$" is the thickness of the PDA layer, "$t3$" is the thickness of the silicon substrate, and "r" is the ZIF-8 arrays' radius. In this modeling, the periodicity of the composite is 1500 nm, and the thickness of the ZIF-8 arrays, PDA layer, and silicon substrate is 200,10, and 260 nm, respectively. And also, the radius of ZIF-8 is 600 nm.

Each material has physical properties that are defined in the software. The silicon refractive index was chosen from the real and imaginary part of the silicon Palik refractive index,[51] the real and imaginary part of the PDA refractive index obtained from ref 52, and also the refractive index of ZIF-8 from ref 53, over the wavelength region of 1.1 to 1.5 μm. In photonic crystal structures, an effective method for reducing the time is simulated in half of the unit cell. The symmetric and asymmetric periodicity boundary conditions applied on the crystal plane (in the x- and y-directions), and perfectly matched layer (PML) boundary conditions are exerted in the z-direction. PML is an absorption boundary condition that waves propagation without interfering with the field inside the simulation area. For decreasing computational time, a mesh clarity was used with 11 nm in the x- and y-direction and 22 nm in the z-direction. There exists a plane wave source for an electromagnetic wave with a range of 1.1 to 1.5 μm in wavelength. The electric field propagates by 1 vol/meter amplitude in the z-direction. In the following, reflection and transmission monitors were used to know how light passes through the structure. Monitors have located in −1.2 and 1.2 μm in the z-direction, respectively. Figure 2 shows the operation of the desired biosensor. After drawing blood, the blood components are separated by a centrifuge in Figure 2A. As can be seen in Figure 2B, white light is passed through the structure, then blood is placed on the

https://dx.doi.org/10.1021/acsabm.0c01586
ACS Appl. Bio Mater. 2021, 4, 1958−1968

component in Figure 2C, and the light passing through the structure is examined again. Figure 2D indicates the transmission wavelength for the photonic crystal without an analyte, while in Figure 2E, it can be seen that the peak wavelength value was shifted by a different analyte.

3. RESULT AND DISCUSSION

The designed biosensor can detect various blood components. Different blood members, including biotin−streptavidin, bovine serum albumin, cytop (polymer), white blood cells, glucose solution (40 mg/100 mL), hemoglobin, blood plasma, polyacrylamide, Sylgard 184, urethane dimethacrylate, and water, were listed with their refractive index in Table 1. The

Table 1. .The Refractive Index of Different Blood Components[17]

analyte	refractive index (nm)
water	1.33
cytop	1.34
plasma blood	1.35
white blood component	1.36
hemoglobin	1.38
glucose	1.4
Sylgard184	1.43
biotin−streptavidin	1.45
polyacrylamide	1.452
bovine serum albumin	1.47
urethane dimethacrylate	1.481

blood sample is dropped on the structure, and the light enters from one side of the photonic crystal and disorients into the structure and blood parts; on the other hand, it becomes apparent from the other side. Related to the refractive index of blood analyte, the duplication of the ray of light will change in the photonic crystal.

Actual blood samples are ready for accurate recognition irrespective of the sensing method. For the photonic crystal-based technique, the processing creates the blood sample homologous with the goal that any sample can be detected accurately even though it is applied in the small space of a nanoarray. The measured refractive index should be higher in contrast to the air situation when substituting air with the analyte. Therefore, dependent changes are expected in the peak wavelength. This method is a fundamental notion for photonic biosensors. The speed of light decreases when passing through the analyte, which has a higher refractive index.[54] This procedure is a well-known method for photonic crystal-based biosensors to obtain resonance wavelength in the presence of air at the sensing site to be used as a reference for the subsequent measurement steps. Following this, the blood samples are exerted for testing an optimized plan and sensing. In the end, this work was compared with the previous designs.

3.1. Optimal Structure. There are many factors for optimizing the proposed structure. The lattice constant "*a*", radius arrays of ZIF-8 "*r*", thickness of the PDA layer "*t*2", and also thickness of the ZIF-8 layer "*t*1" were used for design structure parameters that influenced the performance of the ZIF-8/PDA photonic crystal biosensor. Two modes are considered: mode A and mode B in wavelength axis. Mode A is 1.2 μm, and mode B is 1.45 μm.

3.1.1. The Effects of the Various Lattice Constants on the Transmission Output. The essential parameter in PC structures is the lattice constant, also called the periodicity, which represents the minimum distance between the center of the arrays in the lattice structure that is repeated. The transmission spectrum is based on the different lattice constants, as shown in Figure 3A. The illustration indicates that by increasing the lattice constant from the range of 1.35 to 1.55 μm, concerning mode A, both the transmission intensity and peak wavelength rose from 0.775 to 1.09 and 1.15 to 1.21 μm, respectively. In contrast, in mode B, as indicated, there are fluctuating trends. In the low periodicity, the transmission intensity is very low and not even in Figure 3A.

3.1.2. The Effects of the Various Radii of the ZIF-8 Arrays on the Transmission Output. Figure 3B shows the transmission output wavelength of the structure based on the different values of the radius of the ZIF-8 arrays. As indicated, between the range of 450 and 650 nm in radius value, by increasing the radius of the ZIF-8, the transmission intensity and peak wavelength value rose in mode A from 0.82 to 1.1 μm and 1.16 to 1.21 μm, respectively. That is different from mode B, and transmission intensity declined with the slump of the radius from 0.48 to 0.26 μm; otherwise, the peak wavelength value went up from 1.43 to 1.45 μm.

3.1.3. The Effects of the Various Thicknesses of the ZIF-8 Arrays on the Transmission Output. The different thicknesses of the ZIF-8 in the range of 150 to 350 nm have insignificant effects on the transmission wavelength shift as shown in Figure 3C; likewise, they affect the transmittance intensity more than the transmission wavelength. In mode A, the transmission intensity has gone down with a rise of the thickness of the ZIF-8 from 1.73 to 1.47. The peak wavelength value improved from 1.17 to 1.23 μm. On the contrary, in mode B, the transmission intensity upsurged from 0.23 to 0.7. Similarly, the peak wavelength value increased from 1.45 to 1.46 μm. Based on the Lu and Hupp equation,[37] the refractive index and thickness followed from the below relation:

$$n = \frac{m\lambda}{L2} \tag{4}$$

where "*m*" is an integer number, the refractive index of the layer is "*n*", and the thickness of the coating layer is "*L*"; so the high thickness leads to a low refractive index of the plate.

3.1.4. The Effects of the Various Thicknesses of PDA on the Transmission Output. The changing thickness of the polydopamine has a powerful influence on the transmission wavelength, as shown in Figure 3D. So here it is the impression that the presence of polydopamine and its thickness are more effective than any other factor.[40] The FWHM has negligibly changed to 1 nm, which we exclude. The various thicknesses of the PDA layer have more influence on the sensitivity; thus, the presence of polydopamine in the designed biosensor is a significant factor. The thickness of PDA causes high peak wavelength shifts and can also affect sensitivity. Therefore, for optimizing the structure factors, the thickness of PDA was selected to be 10 nm, and the sensitivity was recalculated again. If the thickness of the PDA chooses high, the peak wavelength shifts will be lower than the initial value, so whatever the thickness of polydopamine selected, the peak wavelength shift is going to be higher, and eventually, the sensitivity will be high. Thus, the chosen thickness of the PDA should be low. The increased thickness of the polydopamine leads to a blueshift in the wavelength. In mode A, the transmission intensity declined from 0.95 to 0.69 similar to reduction in the peak wavelength value from 1.19 to 1.17 μm. However, in

https://dx.doi.org/10.1021/acsabm.0c01586
ACS Appl. Bio Mater. 2021, 4, 1958−1968

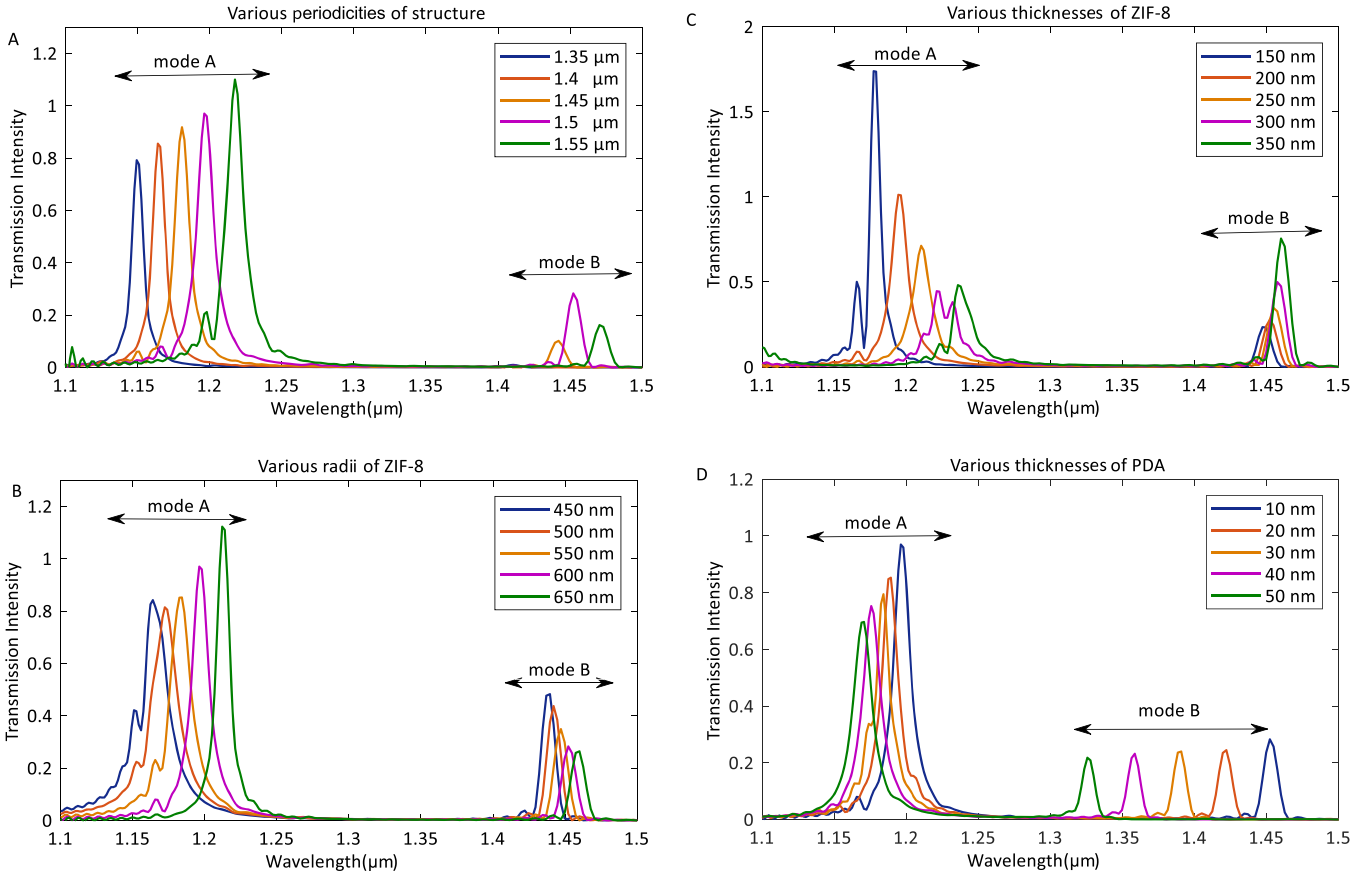

Figure 3. Various factors have been used for the optimized structure. (A) The influence of a variety of periodicities with 1.35, 1.4, 1.45, 1.5, and 1.55 μm as lattice constant "*a*"; (B) result of the change in the radius in the order of 450, 500, 550, 600, and 650 nm as "*r*"; (C) the impact of changing the thickness of ZIF-8 "*t*1", as follows: 150 nm, 200 nm, 250 nm, 300 nm, and 350 nm; (D) the effect of varying the thickness of PDA "*t*2", as follows: 10, 20, 30, 40, and 50 nm.

mode B, the transmission intensity dipped slowly from 0.25 to 0.2, and the peak wavelength value was reduced from 1.45 to 1.32 μm.

3.2. Transmission Intensity. Figure 4A illustrated the recorded transmission intensity with the optimum structural parameters at various refractive indexes in the range of 1.33 to 1.481 nm. After the refractive index of different blood components has been tested on the biosensor, the results were obtained on the transmission spectrum. Since each sample had a specific refractive index, we could detect them by measuring the resonance wavelength change of the system. The chart of the transmission monitor is shown in Figure 4A. Notwithstanding, there are two modes. Mode A has been selected for analysis, which is why it has a high transmission intensity, low FWHM, and better FOM in this structure. The peak wavelength shifts ($\Delta\lambda$) have risen with the growth of the refractive index, and the transmission intensity change (ΔI) has decreased with the escalation of the refractive index, as shown in Figure 4A. Figure 4B shows a zoomed-in image of mode A for a better view.

3.3. Testing the Biosensor. Some factors are essential to illustrate the performance of the photonic crystal-based biosensor, such as the sensitivity (S), full width at half-maximum (FWHM), figure of merit (FOM), and peak wavelength value (PWV). The peak wavelength shift is a significant design factor for the photonic crystal-based biosensors without label because the PWV target range can depend on the readout tools. Also, some biomolecules can be damaged by the light's effect at specific wavelengths of light. The sensitivity is obtained based on eq 5:[55]

$$S = \frac{\Delta\lambda}{\Delta n}\left(\frac{\text{nm}}{\text{RIU}}\right) \tag{5}$$

where "S" is the sensitivity, "$\Delta\lambda$" is the wavelength change, and "Δn" is the refractive index change. FOM and FWHM are two significant factors for indicating the characteristics of the photonic crystal label-free biosensors. Figure of merit (FOM) was used to compare the general action of the optical biosensor. It can be estimated using eq 6:[56]

$$\text{FOM} = \frac{S}{\text{FWHM}} \tag{6}$$

Based on the above results, the detection limit for the intended biosensor is 0.004 RIU. Researchers are looking to make photonic crystal-based biosensors that are of low cost, user-friendly, and accessible to all people at any level of literacy for achieving their therapeutic targets. The sensitivity is defined in photonic crystals as the rate of the wavelength changes by the refractive index variations. So the sensitivity depends on the wavelength changes; when peak transmission wavelength shift is high, the sensitivity will be great. The next case is the value of the peak wavelength shift. If the peak wavelength shift is high for the smallest change in the refractive index, it indicates a desirable biosensor. This desirable biosensor has a low FWHM and high FOM. The results of the simulation are shown in Table 2.

https://dx.doi.org/10.1021/acsabm.0c01586
ACS Appl. Bio Mater. 2021, 4, 1958−1968

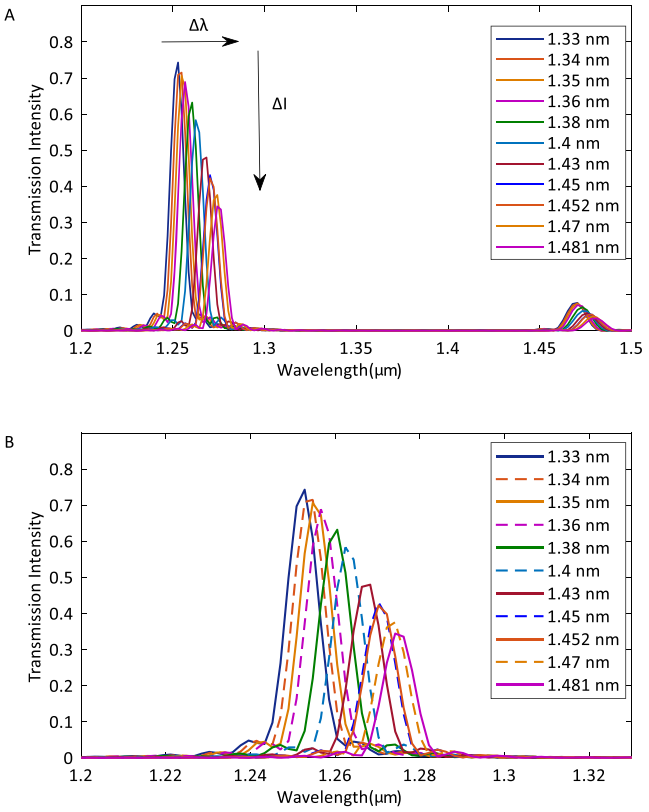

Figure 4. (A) Transmission wavelength shift calculated for air, water, biotin−streptavidin, bovine serum albumin, cytop (polymer), white blood cells, glucose solution (40 mg/100 mL), hemoglobin, blood plasma, polyacrylamide, Sylgard 184, and urethane dimethacrylate by their refractive index: 1, 1.33, 1.34, 1.35, 1.36, 1.38, 1.40, 1.43, 1.45, 1.452, 1.47, and 1.481 nm, respectively. (B) Zoomed-in image of "A" for better visibility. It has a wavelength shift when the refractive index of samples was changed.

According to Table 2, at first sight, when the refractive index increased from 1.33 to 1.481 nm, the peak wavelength value increased from 1.25277 to 1.27416 μm; however, the transmission intensity decreased from 0.743045 to 0.344471. It appears that the sensitivity of the nanostructure declined from 171.51 to 162.14 (nm/RIU) by increasing the refractive indexes. In the case of the FWHM, it is increased from 7.62 to 7.91 nm. The FOM is reduced from 22.50 to 20.49 RIU^{-1} by escalating the FWHM.

For selectivity of the proposed biosensor, two cancer cells are used as the model system. The refractive index of MDA-MB-231 and MCF-7 is 1.399 and 1.401 nm, respectively. Water is selected as a reference in this step, with a refractive index of 1.33 nm. Their results are compared with glucose by a refractive index of 1.4 nm. As it is clear, these analytes have a 0.001 nm difference in their refractive index from each other. Therefore, the peak wavelength values are expected to have moderate shifts. Water, MDA-MB-231, glucose, and MCF-7 are placed on the surface of the suggested platform as analytes. As shown in Figure 5A, the resonance shift cannot be seen as

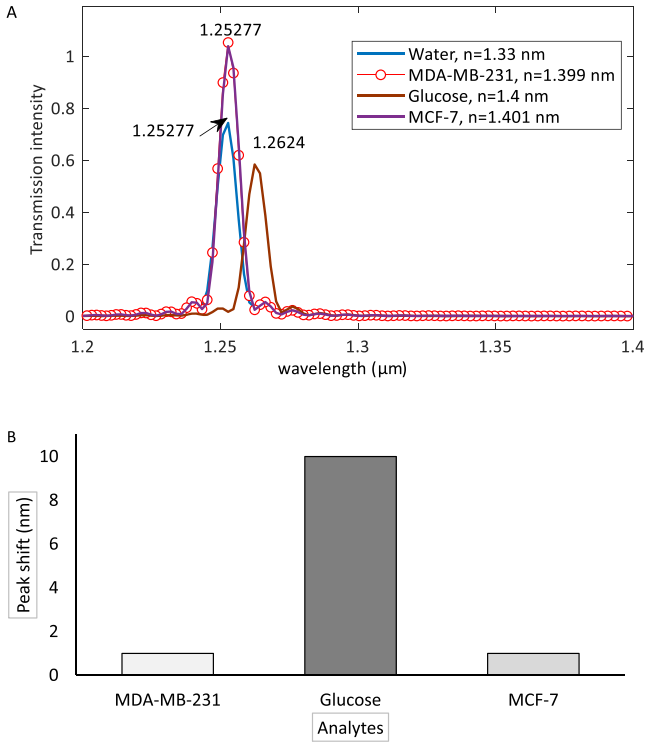

Figure 5. Selectivity of the suggested biosensor. (A) MDA-MB-231 and MCF-7 are placed on the proposed biosensor with the same previous structure for the selectivity test with no peak wavelength shift. (B) With increased thickness of the surface layer, peak wavelength shifted negligibly for MDA-MB-231 and MCF-7.

predicted by MDA-MB-231 and MCF-7. The peak wavelength for water, MDA-MB-231, and MCF-7 is the same at 1.25277 μm, while glucose has a 10 nm peak wavelength shift in 1.2624

Table 2. Measurement of the Transmission Wavelength Intensity for the First and Second Peaks and Their Sensitivity Based on the Refractive Index for the Different Blood Components

analyte	PWV (μm)	T (μm)	S (nm/RIU)	FWHM (nm)	FOM
water	1.25277	0.743045	171.51	7.62	22.50
cytop	1.25468	0.71514	172.08	7.65	22.49
blood plasma	1.25468	0.706588	167.17	7.67	21.79
white blood component	1.2566	0.688982	167.86	7.69	21.82
hemoglobin	1.26046	0.632053	169.18	7.72	21.91
glucose red blood component	1.2624	0.58335	165.57	7.76	21.33
Sylgard184	1.26825	0.479976	167.62	7.81	21.46
biotin−streptavidin	1.27021	0.431277	164.53	7.87	20.90
polyacrylamide	1.27021	0.422516	163.8	7.87	20.81
bovine serum albumin	1.27416	0.375997	165.93	7.89	21.03
urethane dimethacrylate	1.27416	0.344471	162.14	7.91	20.49

https://dx.doi.org/10.1021/acsabm.0c01586
ACS Appl. Bio Mater. 2021, 4, 1958−1968

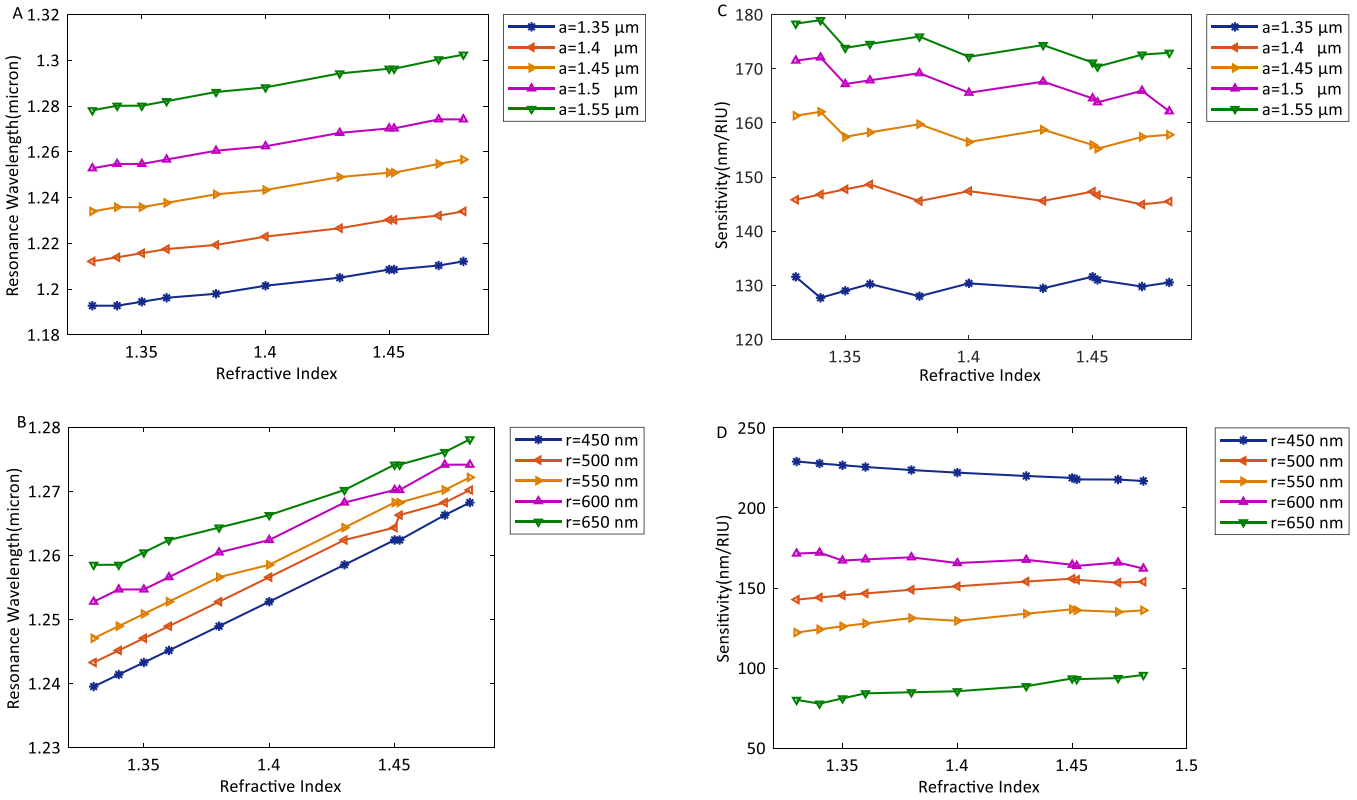

Figure 6. (A) The peak resonance wavelength against the refractive index (nm) changes with the different periodicities. (B) The peak resonance wavelength against the variant refractive index (nm) at a different radius. (C) The sensitivity of the structure in various periodicities over the refractive index variations. (D) The sensitivity of the component over the refractive index change from 1.33 to 1.481 nm for the different radii of ZIF-8.

μm. However, all of the procedures were the same for each analyte. Thus, it can be concluded that this biosensor is not suitable for the intended cancer cells and cannot detect them. After that, the thickness of the surface layer was increased by 5 nm. As shown in Figure 5B, with the enhancement of the thickness, the peak wavelength shifted negligibly, with a 1 nm peak shift for MDA-MB-231 and MCF-7. So with this condition, this biosensor can detect MDA-MB-231 and MCF-7. Although it was expected to be near the peak wavelength of the glucose peak wavelength, this did not happen. So, the thickness of the surface layer and also the analyte size affect the results of the selectivity in biosensors. Therefore, the intended biosensor is only compatible and unique for detecting variant blood components.

In Figure 6A, it is clear that by growing the structure periodicity, the resonance wavelength is redshifted and increased over the variant refractive index from 1.33 to 1.481 nm. Furthermore, it can be deduced that a larger radius of ZIF-8 resulted in longer wavelengths, as shown in Figure 6B. In Figure 6C, by raising the frequency of the nanostructure, the sensitivity versus refractive index is increased from 127 to 180 (nm/RIU). As can be observed in Figure 6D, when the radius of the structure improved, the sensitivity of the proposed component declined.

This design is proper as a wonderful optical biosensor with a high functionality. Changing the refractive index of samples leads to a shifted peak wavelength. The proposed biosensor has an excellent action for detecting samples. The peak wavelength shift indicates that the refractive index increases by the variant refractive index, thus leading to a higher peak wavelength shift, which means that the materials with a higher refractive index are easily detectable. As is known, the materials with a close refractive index have nearby peak wavelength shifts, so it is more challenging to identify materials that have a limited refractive index and require more precision for making a biosensor with extensive changes in the peak wavelength. This suggested that the biosensor does well, so it can be used to diagnose other diseases and even cancer.

Some factors play a significant role in the optical properties of blood components in many medical diagnoses and therapeutic applications, for example, the absorption coefficient "μa" in mm^{-1}, the scattering coefficient "μs" in mm^{-1}, and the anisotropy factor "g";[1] and also, the refractive index is required for the computation of the optical properties related to the wavelength for physiological concentrations of blood components. In this paper, blood plasma was selected for analysis. Based on the topics discussed, it is not necessary to know the viscosity and other physical properties of the various blood components.

The outcomes of Table 3 have presented a nanoarray biosensor with changing refractive index of various blood members, and it used the FDTD numerical method; so the wavelength resonance, sensitivity, and peak wavelength shift were obtained. In this work, the FDTD package has been used, while previous studies on photonic crystal design have used other software such as MEEP and MBP. So depending on how the photonic crystal structure is modeled and also how they are used to analyze it, the method and software are different. Some biosensors are based on the constant dielectric change, but this study is calculated based on the refractive index change. One of

https://dx.doi.org/10.1021/acsabm.0c01586
ACS Appl. Bio Mater. 2021, 4, 1958−1968

Table 3. Comparison between the Previous Literature and This Study about Photonic Biosensors for Blood Component Detection

kinds of the blood components	structure of biosensor	sensitivity (nm/RIU)	transmission peak	year	ref
cytop	photonic crystal-based ring resonator	not available	available	2015	57
blood plasma					
ethanol					
hemoglobin					
glucose solution (40 g/100 mL)					
Sylgard184					
biotin−streptavidin					
polyacrylamide					
bovine serum albumin					
water	photonic crystal waveguide		available	2016	56
blood plasma		5.3265			
WBCs		5.28886			
hemoglobin		5.304			
RBCs		5.699			
biotin−streptavidin		5.95			
water	PC fiber based on ring resonator	55.09021	Not available	2017	20
blood plasma		54.04791			
WBCs		53.72134			
hemoglobin		66.46978			
RBCs		56.05429			
5 g/dL of hemoglobin	dual-core PC fiber	8.013	available	2018	58
10 g/dL of hemoglobin		7.68			
15 g/dL of hemoglobin		8.713			
20 g/dL pf hemoglobin		8.2			
water	photonic crystal-based elliptical ring resonator	not available	available	2019	21
cytop					
blood plasma					
white blood component					
hemoglobin					
red blood component					
Sylgard184					
biotin−streptavidin					
polyacrylamide					
bovine serum albumin					
urethane dimethacrylate					
water	nanocavity with double hole defects	473.38	available	2019	22
cytop		460.03			
blood plasma		449.62			
white blood component		439.85			
hemoglobin		419.48			
red blood component		403.38			
Sylgard184		379.99			
biotin−streptavidin		365.44			
polyacrylamide		364.00			
bovine serum albumin		354.00			
urethane dimethacrylate		347.99			
water	ZIF-8/PDA photonic crystal-based nanoarray biosensors	171.51	available	2020	this work
cytop		172.08			
blood plasma		167.17			
white blood component		167.86			
hemoglobin		169.18			
red blood component		165.57			
Sylgard184		167.62			
biotin−streptavidin		164.53			
polyacrylamide		163.8			
bovine serum albumin		165.93			
urethane dimethacrylate		162.14			

https://dx.doi.org/10.1021/acsabm.0c01586
ACS Appl. Bio Mater. 2021, 4, 1958−1968

the benefits of the designed biosensor is its significant sensitivity of about 171 (nm/RIU), with the rest being less sensitive. The proposed biosensor also has the capability of being a lab-on-a-chip and used in any location. Other biosensors require people with specialized skills and cannot be used in just any location. This biosensor is unlabeled, which can save time and money. It is possible to detect multiple analysts simultaneously, which is a useful feature of this biosensor. Also, it has a low FWHM and high FOM. To sum up, the designed biosensor is in many procedures affordable.

4. CONCLUSION

This paper enables a step for the identification of blood compounds based on a photonic crystal biosensor. The suggested biosensor can precisely and concurrently recognize 10 types of optimally designed blood members. The ZIF-8 arrays placed on the PDA layer coated on the silicon substrate created a photonic crystal-based biosensor that can detect different blood components according to their refractive index with detection limit 0.004 RIU. The physical structure of this biosensor is optimized by varying parameters like the lattice constant, radius, thickness of the ZIF-8, and PDA layer. The performance of the designed biosensor was enhanced by the optimization of the composite, which resulted in a high sensitivity (171 nm/RIU). Following these factors, a significant shift in peak wavelength (80 nm) has appeared for the least refractive index changes (0.01 nm change); furthermore, these results show a low FWHM and a desirable FOM. The transmission wavelength ranges from 1.1 to 1.5 μm, which can be a marker for the detection of biotin−streptavidin, bovine serum albumin, cytop (polymer), red blood cells, glucose (100 mL/40 mg), hemoglobin, blood plasma, polyacrylamide, Sylgard 184, and urethane dimethacrylate. This biosensor can be used as a lab-on-a-chip and unlabeled biosensor with high precision. It is an easy way to detect various blood components and to detect multiple hematological abnormalities. So it is possible to design a biosensor made of MOFs and PDA using the FDTD numerical method to identify compounds in the blood, and a bright future holds out for the use of this structure for the detection of cancer and other diseases.

AUTHOR INFORMATION

Corresponding Author

Amir Razmjou − *Department of Biotechnology, Faculty of Advanced Sciences and Technologies, University of Isfahan, Isfahan 73441-81746, Iran; UNESCO Centre for Membrane Science and Technology, School of Chemical Engineering, University of New South Wales, Sydney, NSW 2052, Australia; Centre for Technology in Water and Wastewater, University of Technology Sydney, Sydney, NSW 2007, Australia;* orcid.org/0000-0002-3554-5129; Email: amirr@unsw.edu.au

Authors

Maryam Nankali − *Department of Biomedical Engineering, North Tehran Branch, Islamic Azad University, Tehran 16511-53311, Iran*

Zahra Einalou − *Department of Biomedical Engineering, North Tehran Branch, Islamic Azad University, Tehran 16511-53311, Iran*

Mohsen Asadnia − *School of Engineering, Macquarie University, Sydney, NSW 2109, Australia;* orcid.org/0000-0003-3157-7796

Complete contact information is available at: https://pubs.acs.org/10.1021/acsabm.0c01586

Notes

The authors declare no competing financial interest.

REFERENCES

(1) Roggan, A.; Friebel, M.; Dörschel, K.; Hahn, A.; Müller, G. Optical properties of circulating human blood in the wavelength range 400-2500 nm. *J. Biomed. Opt.* **1999**, *4*, 36−46.

(2) Mohammad, M.; Razmjou, A.; Liang, K.; Asadnia, M.; Chen, V. Metal-Organic-Framework-Based Enzymatic Microfluidic Biosensor via Surface Patterning and Biomineralization. *ACS Appl. Mater. Interfaces* **2019**, *11*, 1807−1820.

(3) Ejeian, F.; Etedali, P.; Mansouri-Tehrani, H. A.; Soozanipour, A.; Low, Z. X.; Asadnia, M.; Taheri-Kafrani, A.; Razmjou, A. Biosensors for wastewater monitoring: A review. *Biosens. Bioelectron.* **2018**, *118*, 66−79.

(4) Shirani, E.; Razmjou, A.; Tavassoli, H.; Landarani-Isfahani, A.; Rezaei, S.; Abbasi Kajani, A.; Asadnia, M.; Hou, J.; Ebrahimi Warkiani, M. Strategically Designing a Pumpless Microfluidic Device on an "inert" Polypropylene Substrate with Potential Application in Biosensing and Diagnostics. *Langmuir* **2017**, *33*, 5565−5576.

(5) Karimi-Maleh, H.; Alizadeh, M.; Orooji, Y.; Karimi, F.; Baghayeri, M.; Rouhi, J.; Tajik, S.; Beitollahi, H.; Agarwal, S.; Gupta, V. K.; Rajendran, S.; Rostamnia, S.; Fu, L.; Saberi-Movahed, F.; Malekmohammadi, S. Guanine-Based DNA Biosensor Amplified with Pt/SWCNTs Nanocomposite as Analytical Tool for Nanomolar Determination of Daunorubicin as an Anticancer Drug: A Docking/Experimental Investigation. *Ind. Eng. Chem. Res.* **2021**, *60*, 816−823.

(6) Orooji, Y.; Sohrabi, H.; Hemmat, N.; Oroojalian, F.; Baradaran, B.; Mokhtarzadeh, A.; Mohaghegh, M.; Karimi-Maleh, H. An Overview on SARS-CoV-2 (COVID-19) and Other Human Coronaviruses and Their Detection Capability via Amplification Assay, Chemical Sensing, Biosensing, Immunosensing, and Clinical Assays. *Nano-Micro Lett.* **2021**, *13*, 18.

(7) Jalili, R.; Khataee, A.; Rashidi, M. R.; Razmjou, A. Detection of penicillin G residues in milk based on dual-emission carbon dots and molecularly imprinted polymers. *Food Chem.* **2020**, *314*, 126172.

(8) Zhao, Y.; Zhao, X.; Gu, Z. Photonic crystals in bioassays. *Adv. Funct. Mater.* **2010**, *20*, 2970−2988.

(9) Homola, J. Surface plasmon resonance sensors for detection of chemical and biological species. *Chem. Rev.* **2008**, *108*, 462−493.

(10) Blanco, F. J.; Agirregabiria, M.; Berganzo, J.; Mayora, K.; Elizalde, J.; Calle, A.; Dominguez, C.; Lechuga, L. M. Microfluidic-optical integrated CMOS compatible devices for label-free biochemical sensing. *J. Micromech. Microeng.* **2006**, *16*, 1006.

(11) Skivesen, N.; Têtu, A.; Kristensen, M.; Kjems, J.; Frandsen, L. H.; Borel, P. I. Photonic-crystal waveguide biosensor. *Opt. Express* **2007**, *15*, 3169−3176.

(12) Iqbal, M.; Gleeson, M. A.; Spaugh, B.; Tybor, F.; Gunn, W. G.; Hochberg, M.; Baehr-Jones, T.; Bailey, R. C.; Gunn, L. C. Label-free biosensor arrays based on silicon ring resonators and high-speed optical scanning instrumentation. *IEEE J. Sel. Top. Quantum Electron.* **2010**, *16*, 654−661.

(13) Wu, D. K. C.; Kuhlmey, B. T.; Eggleton, B. J. Ultrasensitive photonic crystal fiber refractive index sensor. *Opt. Lett.* **2009**, *34*, 322−324.

(14) Lee, M. R.; Fauchet, P. M. Two-dimensional silicon photonic crystal based biosensing platform for protein detection. *Opt. Express* **2007**, *15*, 4530−4535.

(15) Altug, H. *Physics and applications of photonic crystal nanocavities*; Diss. Stanford University, 2007.

(16) Bohunicky, B.; Mousa, S. A. Biosensors: the new wave in cancer diagnosis. *Nanotechnol., Sci. Appl.* **2011**, *4*, 1.

(17) Sharma, P.; Roy, S. K.; Sharan, P. Design and simulation of photonic crystal based biosensor for detection of different blood components. In *2014 IEEE REGION 10 SYMPOSIUM*; IEEE, 2014; pp 171−176.
(18) Sharma, P.; Sharan, P. Photonic crystal based ring resonator sensor for detection of glucose concentration for biomedical applications. *Int. J. Emerging Technol. Adv. Eng.* **2014**, *4*, 702−706.
(19) Thenmozhi, H.; Rajan, M. S. M.; Devika, V.; Vigneswaran, D.; Ayyanar, N. D-glucose sensor using photonic crystal fiber. *Optik* **2017**, *145*, 489−494.
(20) Singh, S.; Kaur, V. Photonic crystal fiber sensor based on sensing ring for different blood components. In *Design and analysis, 2017 Ninth International Conference on Ubiquitous and Future Networks (ICUFN)*; IEEE, 2017; pp 399−403.
(21) Arunkumar, R.; Suaganya, T.; Robinson, S. Design and analysis of 2D photonic crystal based biosensor to detect different blood components. *Photonic Sens.* **2019**, *9*, 69−77.
(22) Mohammed, N. A.; Hamed, M. M.; Khalaf, A. A. M.; Alsayyari, A.; El-Rabaie, S. High-sensitivity ultra-quality factor and remarkable compact blood components biomedical sensor based on nanocavity coupled photonic crystal. *Results Phys.* **2019**, *14*, 102478.
(23) Karimi-Maleh, H.; Kumar, B. G.; Rajendran, S.; Qin, J.; Vadivel, S.; Durgalakshmi, D.; Gracia, F.; Soto-Moscoso, M.; Orooji, Y.; Karimi, F. Tuning of metal oxides photocatalytic performance using Ag nanoparticles integration. *J. Mol. Liq.* **2020**, *314*, 113588.
(24) Karimi-Maleh, H.; Orooji, Y.; Ayati, A.; Qanbari, S.; Tanhaei, B.; Karimi, F.; Alizadeh, M.; Rouhi, J.; Fu, L.; Sillanpää, M. Recent advances in removal techniques of Cr(VI) toxic ion from aqueous solution: A comprehensive review. *J. Mol. Liq.* **2020**, 115062.
(25) Karimi-Maleh, H.; Shafieizadeh, M.; Taher, M. A.; Opoku, F.; Kiarii, E. M.; Govender, P. P.; Ranjbari, S.; Rezapour, M.; Orooji, Y. The role of magnetite/graphene oxide nano-composite as a high-efficiency adsorbent for removal of phenazopyridine residues from water samples, an experimental/theoretical investigation. *J. Mol. Liq.* **2020**, *298*, 112040.
(26) Mohammad, M.; Lisiecki, M.; Liang, K.; Razmjou, A.; Chen, V. Metal-Phenolic network and metal-organic framework composite membrane for lithium ion extraction. *Appl. Mater. Today* **2020**, *21*, 100884.
(27) Lee, J.; Farha, O. K.; Roberts, J.; Scheidt, K. A.; Nguyen, S. T.; Hupp, J. T. Metal−organic framework materials as catalysts. *Chem. Soc. Rev.* **2009**, *38*, 1450−1459.
(28) Lei, J.; Li, Y.-P.; Xue, Y.-Y.; Wang, Y.; Li, S.-N.; Jiang, Y.-C.; Hu, M.-C.; Zhai, Q.-G. Design of robust rod-packing [In (OH)-(BDC)] frameworks and their high CO2/C2-hydrocarbons over CH4 separation performance. *J. Solid State Chem.* **2019**, *279*, 120936.
(29) Prince, J. A.; Bhuvana, S.; Anbharasi, V.; Ayyanar, N.; Boodhoo, K. V. K.; Singh, G. Self-cleaning Metal Organic Framework (MOF) based ultra filtration membranes-A solution to bio-fouling in membrane separation processes. *Sci. Rep.* **2014**, *4*, 6555.
(30) Razmjou, A.; Asadnia, M.; Hosseini, E.; Habibnejad Korayem, A.; Chen, V. Design principles of ion selective nanostructured membranes for the extraction of lithium ions. *Nat. Commun.* **2019**, *10*, 5793.
(31) Asadniaye Fardjahromi, M.; Razmjou, A.; Vesey, G.; Ejeian, F.; Banerjee, B.; Chandra Mukhopadhyay, S.; Ebrahimi Warkiani, M. Mussel inspired ZIF8 microcarriers: a new approach for large-scale production of stem cells. *RSC Adv.* **2020**, *10*, 20118−20128.
(32) Low, Z. X.; Razmjou, A.; Wang, K.; Gray, S.; Duke, M.; Wang, H. Effect of addition of two-dimensional ZIF-L nanoflakes on the properties of polyethersulfone ultrafiltration membrane. *J. Membr. Sci.* **2014**, *460*, 9−17.
(33) Liu, Q.; Low, Z. X.; Li, L.; Razmjou, A.; Wang, K.; Yao, J.; Wang, H. ZIF-8/Zn_2GeO_4 nanorods with an enhanced CO_2 adsorption property in an aqueous medium for photocatalytic synthesis of liquid fuel. *J. Mater. Chem. A* **2013**, *1*, 11563−11569.
(34) Fairen-Jimenez, D.; Moggach, S. A.; Wharmby, M. T.; Wright, P. A.; Parsons, S.; Düren, T. Opening the gate: framework flexibility in ZIF-8 explored by experiments and simulations. *J. Am. Chem. Soc.* **2011**, *133*, 8900−8902.
(35) Venna, S. R.; Carreon, M. A. Highly permeable zeolite imidazolate framework-8 membranes for CO2/CH4 separation. *J. Am. Chem. Soc.* **2010**, *132*, 76−78.
(36) Guan, Y.; Shi, J.; Xia, M.; Zhang, J.; Pang, Z.; Marchetti, A.; Wang, X.; Cai, J.; Kong, X. Monodispersed ZIF-8 particles with enhanced performance for CO2 adsorption and heterogeneous catalysis. *Appl. Surf. Sci.* **2017**, *423*, 349−353.
(37) Lu, G.; Hupp, J. T. Metal− organic frameworks as sensors: a ZIF-8 based Fabry− Pérot device as a selective sensor for chemical vapors and gases. *J. Am. Chem. Soc.* **2010**, *132*, 7832−7833.
(38) Chen, B.; Yang, Z.; Zhu, Y.; Xia, Y. Zeolitic imidazolate framework materials: recent progress in synthesis and applications. *J. Mater. Chem. A* **2014**, *2*, 16811−16831.
(39) Yang, H.-C.; Wu, M.-B.; Li, Y.-J.; Chen, Y.-F.; Wan, L.-S.; Xu, Z.-K. Effects of polyethyleneimine molecular weight and proportion on the membrane hydrophilization by codepositing with dopamine. *J. Appl. Polym. Sci.* **2016**, *133*, 43792.
(40) Tahroudi, Z. M.; Razmjou, A.; Bagherian, M.; Asadnia, M. Polydopamine surface modification with UV-shielding effect using KMnO4 as an efficient oxidizing agent. *Colloids Surf., A* **2018**, *559*, 68−73.
(41) Liebscher, J.; Mrówczyński, R.; Scheidt, H. A.; Filip, C.; Hădade, N. D.; Turcu, R.; Bende, A.; Beck, S. Structure of polydopamine: a never-ending story? *Langmuir* **2013**, *29*, 10539−10548.
(42) Postma, A.; Yan, Y.; Wang, Y.; Zelikin, A. N.; Tjipto, E.; Caruso, F. Self-polymerization of dopamine as a versatile and robust technique to prepare polymer capsules. *Chem. Mater.* **2009**, *21*, 3042−3044.
(43) Huang, K.-J.; Liu, Y.-J.; Wang, H.-B.; Wang, Y.-Y. A sensitive electrochemical DNA biosensor based on silver nanoparticles-polydopamine@ graphene composite. *Electrochim. Acta* **2014**, *118*, 130−137.
(44) Lee, H.; Rho, J.; Messersmith, P. B. Facile conjugation of biomolecules onto surfaces via mussel adhesive protein inspired coatings. *Adv. Mater.* **2009**, *21*, 431−434.
(45) Batul, R.; Tamanna, T.; Khaliq, A.; Yu, A. Recent progress in the biomedical applications of polydopamine nanostructures. *Biomater. Sci.* **2017**, *5*, 1204−1229.
(46) Razmjou, A.; Asadnia, M.; Ghaebi, O.; Yang, H.-C.; Ebrahimi Warkiani, M.; Hou, J.; Chen, V. Preparation of iridescent 2D photonic crystals by using a mussel-inspired spatial patterning of ZIF-8 with potential applications in optical switch and chemical sensor. *ACS Appl. Mater. Interfaces* **2017**, *9*, 38076−38080.
(47) Nejad, H. E.; Mir, A.; Farmani, A. Supersensitive and tunable nano-biosensor for cancer detection. *IEEE Sens. J.* **2019**, *19*, 4874−4881.
(48) Barnoon, P.; Toghraie, D. Numerical investigation of laminar flow and heat transfer of non-Newtonian nanofluid within a porous medium. *Powder Technol.* **2018**, *325*, 78−91.
(49) Jourabian, M.; Darzi, A. A. R.; Toghraie, D.; Akbari, O. a. Melting process in porous media around two hot cylinders: Numerical study using the lattice Boltzmann method. *Phys. A: Stat. Mech. Appl.* **2018**, *509*, 316−335.
(50) Nemati, M.; Shateri Najaf Abady, A. R.; Toghraie, D.; Karimipour, A. Numerical investigation of the pseudopotential lattice Boltzmann modeling of liquid−vapor for multi-phase flows. *Phys. A: Stat. Mech. Appl.* **2018**, *489*, 65−77.
(51) Benedict, L. X.; Shirley, E. L.; Bohn, R. B. Theory of optical absorption in diamond, Si, Ge, and GaAs. *Phys. Rev. B* **1998**, *57*, R9385.
(52) Zhang, C.; Wu, B.-H.; Du, Y.; Ma, M.-Q.; Xu, Z.-K. Mussel-inspired polydopamine coatings for large-scale and angle-independent structural colors. *J. Mater. Chem. C* **2017**, *5*, 3898−3902.
(53) Van Cleuvenbergen, S.; Stassen, I.; Gobechiya, E.; Zhang, Y.; Markey, K.; De Vos, D. E.; Kirschhock, C.; Champagne, B.; Verbiest,

https://dx.doi.org/10.1021/acsabm.0c01586
ACS Appl. Bio Mater. 2021, 4, 1958−1968

T.; Van Der Veen, M. A. ZIF-8 as nonlinear optical material: influence of structure and synthesis. *Chem. Mater.* **2016**, *28*, 3203−3209.
(54) Datta, A. K.; Munshi, S., *Information photonics: fundamentals, technologies, and applications*. CRC Press: 2016, DOI: 10.1201/9781315373072.
(55) Zhou, J.; Tian, H.; Huang, L.; Fu, Z.; Sun, F.; Ji, Y. Parabolic tapered coupled two photonic crystal nanobeam slot cavities for high-FOM biosensing. *IEEE Photonics Technol. Lett.* **2016**, *29*, 1281−1284.
(56) Chopra, H.; Kaler, R. S.; Painam, B. Photonic crystal waveguide-based biosensor for detection of diseases. *J. Nanophotonics* **2016**, *10*, No. 036011.
(57) Sharma, P.; Sharan, P. Design of photonic crystal based ring resonator for detection of different blood constituents. *Opt. Commun.* **2015**, *348*, 19−23.
(58) Ayyanar, N.; Khalil, A. E.; Hameed, M. F. O.; Raja, G. T.; Obayya, S. S. A. Enhanced sensitivity of hemoglobin sensor using dual-core photonic crystal fiber. *Opt. Quantum Electron.* **2018**, *50*, 453.

https://dx.doi.org/10.1021/acsabm.0c01586
ACS Appl. Bio Mater. 2021, 4, 1958−1968